Journal of Atmospheric and Solar-Terrestrial Physics 179 (2018) 22–33

Contents lists available at ScienceDirect

Journal of Atmospheric and Solar-Terrestrial Physics

journal homepage: www.elsevier.com/locate/jastp

Possibility of simultaneous [O_3] and [CO_2] altitude distribution retrievals from the daytime emissions of electronically-vibrationally excited molecular oxygen in the mesosphere

Valentine Yankovsky*, Rada Manuilova

Atmospheric Physics Department, Saint Petersburg State University, Saint Petersburg, Russia

A B S T R A C T

In this study we have formulated the multi-channel method for retrieval of the $O(^3P)$, O_3 and CO_2 volume mixing ratios, $C_{v,O(3P)}$, $C_{v,O3}$ and $C_{v,CO2}$, altitude profiles in the daytime mesosphere and lower thermosphere from the simultaneous measurements of intensities of three emissions formed by transitions from three electronically-vibrationally excited states, $O_2(b^1\Sigma_g^+, v = 2)$, $O_2(b^1\Sigma_g^+, v = 1)$ and $O_2(b^1\Sigma_g^+, v = 0)$. Only using the YM2011 model of kinetics of O_3 and O_2 photolysis (Yankovsky et al., 2016. J. Molec. Spectr., 327, 209–232) allowed us to consider in detail the complex groups of the processes of excitation and quenching of the states $O_2(b^1\Sigma_g^+, v = 0, 1, 2)$, the transitions from which form the system of the O_2 Atmospheric bands observed in the dayglow of the Earth. For the altitude range 50–85 km we developed in details the two-channel method of simultaneously retrieval of the volume mixing ratios of O_3 and CO_2. For this method, we succeeded in obtaining formulas that can be used for remote sensing of the Earth atmosphere from satellites.

1. Introduction

The small components of the Earth daytime mesosphere and lower thermosphere (MLT), carbon dioxide, ozone and atomic oxygen are responsible for the thermal regime in the MLT region, so the knowledge about the altitude dependences of the concentrations of these components is very important. (e.g. López-Puertas and Taylor, 2001; Brasseur and Solomon, 2005; Mlynczak et al., 2007; Feofilov and Kutepov, 2012; Timofeyev, 2016). The altitude profile of carbon dioxide concentration can be measured by a direct method of absorbing radiation from the Sun (Beagley et al., 2010). However, this solar occultation method could be realized only in the conditions of sunset and sunrise, so it cannot give a comprehensive presentation of the altitude profile of the [CO_2] throughout the daytime hours.

The history of the [CO_2] measurements in MLT is well described in (Jurado-Navarro et al., 2016). We will review the recent experiments that made available the satellite [CO_2] datasets. The Sounding of the Atmosphere using Broadband Emission Radiometry (SABER) instrument on board the Thermosphere- Ionosphere-Mesosphere-Energetics and Dynamics (TIMED) satellite has been providing global, simultaneous measurements of limb radiance in 10 spectral channels since January 2002 and, in particular, has been measuring the atmospheric limb radiance in the 15 μm and 4.3 μm channels. In (Rezac et al., 2015) the authors present a methodology for a self-consistent simultaneous retrieval of kinetic temperature/pressure, T(p) (in the 15 μm channel) and [CO_2] (in 4.3 μm channel) from the broad band infrared limb measurements. The method used for the CO_2 volume mixing ratio (VMR), $C_{v,CO2}$, retrieval considered the complicated non-LTE problem, that is solving the coupled system of kinetic equilibrium and the radiative transfer equations. Using the methodology developed for interpretation SABER measurements by Rezac et al. (2015), Yue et al. (2015) produced a database of the daytime [CO_2] in the MLT region for 13 years. Jurado-Navarro et al. (2016) describe the retrieval of CO_2 VMR from MIPAS (Michelson Interferometer for Passive Atmospheric Sounding) high resolution limb emission spectra in the 4.3 μm region in the interval 70–142 km for 7 years (2005–2012). The $C_{v,CO2}$ have been retrieved using MIPAS daytime limb emission spectra in the 4.3 μm band from January 2005 until March 2012. The Fourier Transform Spectrometer on the Canadian Atmospheric Chemistry Experiment ACE-FTS (Beagley et al., 2010) has measured the $C_{v,CO2}$ in the mesosphere and lower thermosphere (70–120 km) by using the solar occultation technique. The latter method has an advantage because it is free from non-LTE effects and necessity to solve the complicated problem of radiative transfer at non-LTE conditions for the [CO_2] retrieval, but, as it was mentioned above, provides a limited time coverage (Beagley et al., 2010).

* Corresponding author.
E-mail address: vyankovsky@gmail.com (V. Yankovsky).

https://doi.org/10.1016/j.jastp.2018.06.008
Received 25 February 2018; Received in revised form 6 June 2018; Accepted 12 June 2018
Available online 13 June 2018
1364-6826/

The former observations of CO_2 in the middle atmosphere showed a rapid falloff above about 80 km (e.g. (Kauffmann et al., 2002; Feofilov and Kutepov, 2012)) and the recent measurements made by the SABER, ACE and MIPAS instruments mentioned above has confirmed this fact (Rezac et al., 2015; Yue et al., 2015; Jurado-Navarro et al., 2016). It should be noted that, as it shown in (Emmert et al., 2012; Garcia et al., 2014; Rezac et al., 2015; Yue et al., 2015; Qian et al., 2017) the SABER and ACE-FTS $[CO_2]$ altitude profiles demonstrate a faster increase of the $[CO_2]$ above 80 km for 10 years, compared to SD-WACCM model. The SABER CO_2 trend shows a peak at ~110 km of about 12% per decade.

A comprehensive review of the $[O_3]$ measurement methods (Smith et al., 2013) serves to analyze the discrepancies between several experiments, such as HALOE, HRDI, MIPAS, GOMOS, ACE-FTS, SOFIE, OSIRIS, SMILES and TIMED-SABER. In (Yankovsky and Manuilova, 2017) we have compared the $[O_3]$ retrieval from SABER measurements of the 1.27 μm emission intensity in the framework of two models of O_3 and O_2 photolysis: YM2011 model of electronic – vibrational kinetics (Yankovsky et al., 2016) and the model of pure electronic kinetics developed by Mlynczak, Solomon and Zaras in (Mlynczak et al., 1993) with the $[O_3]$ measured by the following instruments: High Resolution Doppler Imager (HRDI) on the UARS satellite; MIPAS on the Envisat satellite; the SMILES superconducting submillimeter radiometer at the International Space Station. The comparison of the $[O_3]$ profiles obtained in (HRDI), SMILES and MIPAS experiments shows that retrieval of the $[O_3]$ in the framework of YM2011 model is close to these data. In (Yankovsky and Manuilova, 2017) we have shown that in order to retrieve the $[O_3]$ altitude profile from the measurements of the intensity of the O_2 band in the region of 1.27 μm correctly, it is necessary to use the photochemical model of the electronic-vibrational kinetics of excited products of ozone and oxygen photolysis in the mesosphere and lower thermosphere YM2011. In (Martyshenko and Yankovsky, 2017) in the framework of YM2011 model we have derived the formulas for the $[O_3]$ retrieval from the measurements of volume emission rate (VER) in the 1.27 μm O_2 Atmospheric band (0, 0) for the range 50–85 km.

In (Yankovsky et al., 2016) we developed the methods of simultaneous retrieval of ozone and atomic oxygen altitude profiles above the mesopause using as proxies electronically - vibrationally excited levels of oxygen molecule, namely $O_2(b^1\Sigma_g^+, v = 0, 1, 2)$, $O_2(a^1\Delta_g, v = 0, 1)$ and excited atom $O(^1D)$.

In (Yankovsky, 2017) in the framework YM2011 model, we have investigated the possibilities of retrieval the $[O_3]$ and $[CO_2]$ altitude profiles. Note, that for all these excited states the rate coefficients of quenching in collisions with CO_2 molecules have been measured.

In this study we suggest method of the $[CO_2]$ retrievals in the range 50–85 km and discuss the possibility of the $[O_3]$ and $[CO_2]$ simultaneous retrieval in the altitude range 85–100 km. The method developed here can be used during the whole daytime and does not require the solution of complex problems of radiation transfer in the case of LTE breaking. We have got the applied formulas for the simultaneous retrieval of the volume mixing ratios of CO_2 and O_3 that can be used for remote sensing of the Earth atmosphere from satellites.

In Section 2 we considered briefly the extended YM2011 model of kinetics of the products of O_2 and O_3 photodissociation in the MLT and discussed the model which we use for the present study, and also presented the survey of the rate coefficients. In the present study we took into account 6 levels from 45 levels of whole YM2011. In Section 3 we investigated the quenching factors for all excited specious under consideration. In Section 4 we gave the solution of the forward problem: the calculations of the altitude profiles of $[O_2(b^1\Sigma_g^+, v = 0)]$, $[O_2(b^1\Sigma_g^+, v = 1]$, $[O_2(b^1\Sigma_g^+, v = 2)]$ and $[O(^1D)]$. In Section 5 we presented an analytical solution of the inverse kinetic problem for the $[CO_2]$ retrieval in the mesosphere. In Section 6 we carried out analysis of the complete formulas for retrieving the altitude dependences of the CO_2 and O_3 volume mixing ratios in the mesosphere. In Section 7 we made analysis of the new method of simultaneous retrieval of the CO_2 and O_3 volume mixing ratios in the mesosphere which enabled us to get the simple analytical formulas for the $[CO_2]$ and $[O_3]$ retrievals from the intensities of the emissions in the corresponding O_2 Atmospheric bands. In Section 8 we discussed the proposal on the three-channel method of simultaneous retrieval of the volume mixing ratios profiles of three components, $O(^3P)$, O_3, CO_2, in the altitude range of 85–100 km. In Section 9 we presented the main conclusions.

2. Model of photochemical kinetics YM2011

In the extended YM2011 model of kinetics of the products of O_2 and O_3 photodissociation in the MLT, we consider the kinetic balance equations for 45 levels: three electronically-vibrationally excited levels $O_2(b^1\Sigma_g^+, v \le 2)$, six levels $O_2(a^1\Delta_g, v \le 5)$, 35 levels $O_2(X^3\Sigma^-_g, v \le 35)$ and level $O(^1D)$ (Yankovsky et al., 2016). As the sources of O (^1D) in MLT, besides the O_3 photolysis in the spectral Hartley and Huggins bands (λ = 200–370 nm), we also considered the photolysis of O_2 in the Schumann-Runge continuum (λ = 120–174 nm) and H Lyman-α line. The quantum yields of $O(^1D)$ formation were taken from (Sander et al., 2011). Note, that the quantum yield of $O(^1D)$ in the Huggins band is very small in comparison with the quantum yield in the Hartley band and is equal to 0.08 ± 0.04 in the interval λ = 329–340 nm independent of temperature, and for λ > 340 nm there are no recommendations for it (Sander et al., 2011).

All electronically-vibrationally excited levels are depopulated by V–V (vibrational – vibrational) and V–T (vibrational – translational) energy exchange processes in collisions with O_2, N_2, $O(^3P)$, O_3 and CO_2 molecules. The system of kinetic balance equations considers the populations of all 45 states taking into account.

For our purpose we use the part of YM2011 model and take into account 10 levels: three levels $O_2(b^1\Sigma_g^+, v = 0,1, 2)$, six levels $O_2(a^1\Delta_g, v = 0–5)$ and level $O(^1D)$ (Fig. 1). It is enough for description of mechanisms of emissions in the molecular oxygen Atmospheric and IR Atmospheric bands. We consider more than 60 radiative quenching and photoexcitation processes and processes of deexcitation by V–V and V–T energy exchange in collisions. For comparison, in the entire YM2011 model one should take into consideration more than 150 processes (Yankovsky et al., 2011).

In this study all possible processes of energy transfer between the excited levels have been taken into account, and Appendix 1 of (Yankovsky et al., 2016) contains an overview of currently available kinetic data concerning all 60 above mentioned reactions. We present the compilation of kinetic data for 10 excited oxygen species, namely, for the energy transfer processes, which take place at collisions of the electronically-vibrationally excited molecules $O_2(b^1\Sigma_g^+, v = 0, 1, 2)$ and $O_2(a^1\Delta_g, v = 0–5)$ and oxygen atom $O(^1D)$ with the main atmospheric components O (^3P), O_2, N_2, O_3 and CO_2. We used the measured values of the reaction rate coefficients and quantum yields of the excited products that were obtained mainly for the last 15 years (Table A1.1. in (Yankovsky et al., 2016)).

In Table 1 we present an updated version of this database on the rate coefficients of quenching of the following six levels: $O_2(b^1\Sigma_g^+, v = 0, 1, 2)$, $O_2(a^1\Delta_g, v = 0, 1)$ and level $O(^1D)$. Table 1 takes into account the measurements of the values of the rate coefficients and of the radiative lifetimes of the excited levels that appeared over the past three years. In the Table 1 the room temperature, RT, corresponds to the interval 290–300 K.

3. Investigations of the quenching factor for six proxies

In general, the kinetic equation for the concentration of excited component, x_m, looks like:

$$\frac{\partial [x_m]}{\partial t} = P(x_m) - [x_m]Q(x_m) \quad (1)$$

Table 1
The rate coefficients for reactions involving $O(^1D)$, $O_2(b^1\Sigma_g^+, v = 0–2)$, $O_2(a^1\Delta_g, v = 0, 1)$ in the processes of radiative quenching and deexcitation at collisions with O (^3P), O_2, O_3, N_2, CO_2. The updated version of data base which have been presented in (Yankovsky et al., 2016).

Reaction or radiative quenching processes	Notation of the rate coefficient, *k*, and radiative lifetime, τ	The values of *k*, cm^3s^{-1}, and τ, s	Temperature range, K; et RT – room temperature	Relative uncertainty, ξ, at RT	Notes: the references are presented only for the new data
$O(^1D) \rightarrow O(^3P) + h\nu$	$\tau_{O(1D)}$	110.0			
$O(^1D) + O(^3P) \rightarrow O(^3P) + O(^3P)$	*k(O(1D);O)*	$2.2{\cdot}10^{-11}$	RT	0.27	
$O(^1D) + O_2 \rightarrow O(^3P) + O_2(b^1\Sigma_g^+, v \le 1)$	*k(O(1D);O2)*	$3.10{\cdot}10^{-11}exp$ (87/T)	195–673	0.10	
$O(^1D) + O_3 \rightarrow O_2 + O_2$ [#]	*k(O(1D);O3)*	$2.4{\cdot}10^{-10}$	210–370	0.20	
$O(^1D) + N_2 \rightarrow O(^3P) + N_2(X^1\Sigma_g^+, v \le 7)$	*k(O(1D);N2)*	$2.20{\cdot}10^{-11}exp$ (118/T)	195–673	0.09	
$O(^1D) + CO_2 \rightarrow CO + O_2$	*k(O(1D);CO2)*	$7.5{\cdot}10^{-11}exp$ (115/T)	200–350	0.15	
$O_2(b^1\Sigma_g^+, v = 2) \rightarrow O_2(X^3\Sigma_g^-, v'') + h\nu$	$\tau_{O2(b,2)}$	11.8			(Yu et al., 2014)[a]
$O_2(b^1\Sigma_g^+, v = 2) + O(^3P) \rightarrow O_2(b^1\Sigma_g^+, v' < 2) + O(^3P)$	*k(O2(b, v=2);O)*	$1.07{\cdot}10^{-11}$	340–445	0.6	
$O_2(b^1\Sigma_g^+, v = 2) + O_2 \rightarrow O_2(X^3\Sigma_g^-, v = 2) + O_2(b^1\Sigma_g^+, v = 0)$	*k(O2(b, v=2);O2)*	$2.3{\cdot}10^{-11}exp$ (-691/T)	110–295	0.25	
$O_2(b^1\Sigma_g^+, v = 2) + O_3 \rightarrow 2O_2 + O$	*k(O2(b, v=2);O3)*	$2.9{\cdot}10^{-10}$	340–445	0.4	
$O_2(b^1\Sigma_g^+, v = 2) + N_2 \rightarrow O_2(b^1\Sigma_g^+, v = 0) + N_2(X^1\Sigma_g^+, v = 1)$	*k(O2(b, v=2);N2)*	$8.0{\cdot}10^{-15}$	110	0.4	
$O_2(b^1\Sigma_g^+, v = 2) + CO_2 \rightarrow O_2(b^1\Sigma_g^+, v = 1) + CO_2(100)$	*k(O2(b, v=2);CO2)*	$3.0{\cdot}10^{-12}exp$ (-158/T)	220–295	0.9	
$O_2(b^1\Sigma_g^+, v = 1) \rightarrow O_2(X^3\Sigma_g^-, v'') + h\nu$	$\tau_{O2(b,1)}$	11.4			(Yu et al., 2014)[a]
$O_2(b^1\Sigma_g^+, v = 1) + O(^3P) \rightarrow O_2 + O$	*k(O2(b, v=1);O)*	$4.5{\cdot}10^{-12}$	RT	0.18/-0.29	
$O_2(b^1\Sigma_g^+, v = 1) + O_2 \rightarrow O_2(X^3\Sigma_g^-, v = 1) + O_2(b^1\Sigma_g^+, v = 0)$	*k(O2(b, v=1);O2)*	$4.2{\cdot}10^{-11}exp$ (-312/T) $2.2{\cdot}10^{-11}$ (T/292)*exp* (-115/T)	125–295 292–1000	0.026 (at 295 K) 0.038 (at 292 K)	(Hwang et al., 1999) see Fig. 5 and text
$O_2(b^1\Sigma_g^+, v = 1) + CO_2 \rightarrow O_2(b^1\Sigma_g^+, v = 0) + CO_2(100)$	*k(O2(b, v=1);CO2)*	$9{\cdot}10^{-13}$	220	0.6	
$O_2(b^1\Sigma_g^+, v = 0) \rightarrow O_2(X^3\Sigma_g^-, v'') + h\nu$	$\tau_{O2(b,0)}$	11.0			(Yu et al., 2014)[a]
$O_2(b^1\Sigma_g^+, v = 0) + O(^3P) \rightarrow O_2 + O$	*k(O2(b, v=0);O)*	$8{\cdot}10^{-14}$	RT	0.25	
$O_2(b^1\Sigma_g^+, v = 0) + O_2 \rightarrow O_2(a^1\Delta_g, v'' = 3\text{-}v') + O_2(a^1\Delta_g, v')$	*k(O2(b, v=0);O2)*	$4.10{\cdot}10^{-17}$ $1.3{\cdot}10^{-15}$ (T/292)$^{0.5}$ *exp* (-1105/T)	RT 297–800	0.5 0.21 [b]	 (Zagidullin et al., 2017)
$O_2(b^1\Sigma_g^+, v = 0) + O_3 \rightarrow 2O_2 + O$	*k(O2(b, v=0);O3)*	$3.5{\cdot}10^{-11}exp$ (-135/T)	210–370	0.15	
$O_2(b^1\Sigma_g^+, v = 0) + N_2 \rightarrow O_2(a^1\Delta_g, v = 2) + N_2(X^1\Sigma_g^+, v = 1)$ $\rightarrow O_2(X^3\Sigma_g^-, v = 9) + N_2(X^1\Sigma_g^+, v = 0)$	*k(O2(b, v=0);N2)*	$2.20{\cdot}10^{-15}$ $4.0{\cdot}10^{-16}$ (T/292)$^{1.5}$ *exp* (503/T)	203–373 297–800	0.11 0.08 [b]	see Fig. 4 and text (Zagidullin et al., 2017)
$O_2(b^1\Sigma_g^+, v = 0) + CO_2 \rightarrow O_2(a^1\Delta_g, v = 0) + CO_2$	*k(O2(b, v=0);CO2)*	$4.40{\cdot}10^{-13}$ $5.9{\cdot}10^{-14}$ (T/292)$^{1.5}$ *exp* (595/T)	245–362 297–800	0.10 0.10 [b]	see Fig. 3 and text (Zagidullin et al., 2017)
$O_2(a^1\Delta_g, v = 1) \rightarrow O_2(X^3\Sigma_g^-, v'') + h\nu$	$\tau_{O2(a,1)}$	$4.52{\cdot}10^{3}$			(Yu et al., 2014) [a]
$O_2(a^1\Delta_g, v = 1) + O_2 \rightarrow O_2(X^3\Sigma_g^-, v = 1) + O_2(a^1\Delta_g, v = 0)$	*k(O2(a, v=1);O2)*	$5.6{\cdot}10^{-11}$	RT	0.20	
$O_2(a^1\Delta_g, v = 1) + O_3 \rightarrow 2O_2 + O$	*k(O2(a, v=1);O3)*	$4.7{\cdot}10^{-12}$	RT	0.43	
$O_2(a^1\Delta_g, v = 1) + CO_2 \rightarrow products$	*k(O2(a, v=1);CO2)*	$1.9{\cdot}10^{-14}$	RT	0.11	(Torbin et al., 2017)
$O_2(a^1\Delta_g, v = 0) \rightarrow O_2(X^3\Sigma_g^-, v'') + h\nu$	$\tau_{O2(a,0)}$	$4.40{\cdot}10^{3}$			(Yu et al., 2014) [a]
$O_2(a^1\Delta_g, v = 0) + O(^3P) \rightarrow products$	*k(O2(a, v=0);O)*	$1{\cdot}10^{-16}$	RT	2.0/-0.7	
$O_2(a^1\Delta_g, v = 0) + O_2 \rightarrow O_2(X^3\Sigma_g^-, v'' = 5\text{-}v') + O_2(X^3\Sigma_g^-, v')$	*k(O2(a, v=0);O2)*	$3.6{\cdot}10^{-18}exp$ (-220/T)	100–450	0.20	
$O_2(a^1\Delta_g, v = 0) + O_3 \rightarrow 2O_2 + O$	*k(O2(a, v=0);O3)*	$5.2{\cdot}10^{-11}exp$ (-2840/T)	280–360	0.25	
$O_2(a^1\Delta_g, v = 0) + CO_2 \rightarrow products$	*k(O2(a, v=1);CO2)*	$\le 2{\cdot}10^{-20}$	RT		

[a] The values of **τ** were estimated using the Franck-Condon factors (Yu et al., 2014) and were normalized on the Einstein coefficients $A_{O2(b,v=0 \rightarrow X,\ v=0)} = 0.085\ s^{-1}$ and $A_{O2(b,v=0 \rightarrow a,\ v=0)} = 1.5{\cdot}10^{-3}s^{-1}$ (Krupenie, 1972), $A_{O2(a,v=0 \rightarrow X,\ v=0)} = 2.26{\cdot}10^{-4}\ s^{-1}$ (Newman et al., 2000).

[b] We use the method described in Appendix 1 to calculate the value of the relative uncertainty ξ of the rate coefficient if the authors give the values of the rate coefficients in the Arrhenius form with individual error values for each parameter $k(T) = (A \pm \Delta A)(T/292)^{n \pm \Delta n}exp((b \pm \Delta b)/T)$.

where $P(x_m)$ – the production rate of x_m. In this study x_m are $O(^1D)$, $O_2(b^1\Sigma_g^+, v = 0, 1, 2)$ and $O_2(a^1\Delta_g, v = 0–5)$, $Q(x_m)$ – the quenching factor of x_m:

$$Q(x_m) = (\tau_m)^{-1} + [O_2]k(x_m;O_2) + [O(^3P)]k(x_m;O(^3P)) + [O_3]k(x_m;O_3) + [N_2]k(x_m;N_2) + [CO_2]k(x_m;CO_2) \quad (2)$$

where τ_m – the radiative lifetime of x_m component, $k(x_m; y_j)$ – the rate coefficient of the quenching reaction of component x_m in collision with the main atmospheric components y_j. In this study y_j are O_2, $O(^3P)$, N_2, O_3 and CO_2.

We examine the quenching factors of six components $O(^1D)$, $O_2(b^1\Sigma_g^+, v = 0, 1, 2)$ and $O_2(a^1\Delta_g, v = 0, 1)$. As it was shown in (Yankovsky et al., 2016) the levels O_2 ($a^1\Delta_g$, v = 2–5) do not contribute significantly in populating the level $O_2(a^1\Delta_g, v = 0)$. Fig. 2 (a–f) demonstrates the relative contributions of the deexcitation processes to the quenching factor (2) depending on altitude for all proxies for typical SABER event.

The important conclusion from Fig. 2d is as follows: $O_2(b^1\Sigma_g^+, v = 0)$ – is the single proxy, that is sensitive to variations of the carbon dioxide density in the MLT range. In the altitude range of 60–85 km, quenching of $O_2(b^1\Sigma_g^+, v = 0)$ occurs mainly in collisions with N_2 (the concentration and the rate coefficient of collisions are well known) and partly with CO_2. Below 80 km quenching in collisions with CO_2 contributes near 10% to the quenching factor of $O_2(b^1\Sigma_g^+, v = 0)$. Below 60 km, in addition to N_2 and CO_2 it is necessary to take into account quenching in collisions with O_3.

It is worth emphasizing, that collisions with CO_2 don't take part in the population of the excited levels under consideration. Thus, we are interested in the population of the level $O_2(b^1\Sigma_g^+, v = 0)$, which, as seen from Fig. 1, is populated by the transfer of energy from the $O(^1D)$

atom to the levels $O_2(b^1\Sigma_g^-, v = 0, 1)$, as well as due to the resonance absorption of solar radiance.

4. Solution of the forward kinetic problem

A full system of kinetic equations for the forward problem of determining the populations of the excited levels of the oxygen molecule is presented in (Yankovsky et al., 2016). Note that, in accordance with the conclusions of this work, in calculations of the population of the level $O_2(b^1\Sigma^+_g, v = 0)$, it is necessary to take into account transitions from all higher levels, namely, $O_2(b^1\Sigma^+_g, v = 2)$, $O_2(b^1\Sigma^+_g, v = 1)$ and $O(^1D)$. The contribution of collisional energy transition $O_2(b^1\Sigma_g{}^+, v = 2) + O_2 \rightarrow O_2(X^3\Sigma_g^-, v = 2) + O_2(b^1\Sigma_g, v = 0)$ to the population of the level $O_2(b^1\Sigma_g{}^+, v = 0)$ is less than 0.1% in comparison with the total contribution of transitions $O(^1D) + O_2 \rightarrow O(^3P) + O_2(b^1\Sigma_g{}^+, v \le 1)$, $O_2(b^1\Sigma_g{}^+, v = 2) + O \rightarrow O_2(b^1\Sigma_g{}^+, v = 0) + O$ and of the process of resonant photoexcitation of $O_2(b^1\Sigma_g^-, v = 0)$ (Yankovsky et al., 2016), so the contribution of this transition can be neglected.

We have considered the system of balance equations in the stationary approximation for the populations of four levels, $O(^1D)$, $O_2(b^1\Sigma_g{}^+, v = 0, 1, 2)$ and obtained the expressions for calculations of the proxy concentrations:

$$\left[O(^1D)\right] = \frac{[O_3]J_{HHb}F(O_3 \rightarrow O(^1D); HHb) + [O_2](J_{SRC} + J_{Ly\alpha}F(O_2 \rightarrow O(^1D); Ly\alpha))}{Q(O(^1D))} \quad (3)$$

$$[O_2(b^1\Sigma_g^+,\ v = 2)] = [O_2]\frac{g_\gamma}{Q(O_2(b^1\Sigma_g^+,\ v = 2))} \quad (4)$$

$$[O_2(b^1\Sigma_g^+,\ v = 1)] = [O_2]\frac{g_\beta + [O(^1D)]k(O(^1D); O_2)\Psi_1}{Q(O_2(b^1\Sigma_g^+,\ v = 1))} \quad (5)$$

$$[O_2(b^1\Sigma_g^+,\ v = 0)] = [O_2]\frac{(g_\alpha + [O(^1D)]k(O(^1D); O_2)\Psi_0 + [O_2(b^1\Sigma_g^+,\ v = 1)]k(O_2(b, v = 1); O_2))}{Q(O_2(b^1\Sigma_g^+,\ v = 0))} \quad (6)$$

In formulas (3-6) J_{HHb} – the rate of O_3 photolysis in the Hartley and Huggins bands, $F(O_3 \rightarrow O(^1D); HHb)$ – quantum yield of production of $O(^1D)$ in this process; J_{SRC} and $J_{Ly\alpha}$ – the rate of O_2 photolysis in the Schumann-Runge continuum and H Lyman-α line, and $F(O_2 \rightarrow O(^1D); Ly\alpha)$ – quantum yield of $O(^1D)$ in the last process; Ψ_1 is the quantum yield of $O_2(b^1\Sigma_g^-, v = 1)$ production and Ψ_0 is the quantum yield of $O_2(b^1\Sigma_g^-, v = 0)$ production in reaction $O(^1D) + O_2 \rightarrow O(^3P) + O_2(b^1\Sigma_g^-, v)$, with $\Psi_1 = 0.80 \pm 0.10$ and $\Psi_0 = 0.20 \pm 0.10$ [1]. Parameters g_α, g_β, g_γ are the rates of resonant photoexcitation of $O_2(b^1\Sigma_g^-, v = 0)$, $O_2(b^1\Sigma_g^-, v = 1)$ and $O_2(b^1\Sigma_g^-, v = 2)$ due to absorption of solar radiation, correspondingly.

The denominators, $Q(x_m)$, present the quenching factors of corresponding levels (2). In the atmospheric layer of 50–85 km, the system (3-6) can be simplified, because, as shown by the sensitivity analysis presented in Section 5.1 in (Yankovsky et al., 2016) reactions involving atomic oxygen and O_2 photoabsorption in the Schumann-Runge continuum can be neglected.

5. Analytical solution of the inverse kinetic problem for the [CO_2] retrieval in the mesosphere and the rate coefficients survey

In the altitude range 50–85 km under the conditions of the homosphere, the volume mixing ratios $C_{v,N2}$ and $C_{v,O2}$ for the main atmospheric constituents N_2 and O_2 are practically constant, therefore in formulas (3-6) we take them into account as invariants, and possible uncertainties of the solution of the forward problem we associate with the errors of the values of the reaction rate coefficients of the energy transfer processes between the excited levels O (^{1}D) and $O_2(b^1\Sigma_g{}^+, v = 0, 1, 2)$. Taking this into account, and also expressing the quenching coefficients for $O_2(b^1\Sigma^+_g, v = 0)$ and $O_2(b^1\Sigma^+_g, v = 1)$ in explicit form with the help of (2), from the balance equations (3, 5, 6), we obtain an expression for the CO_2 volume mixing ratio in the altitude range of 50–85 km:

$$C_{v,CO2} = C_{v,O2}\frac{g_\alpha - g_\beta(\Psi_0/\Psi_1) + [O_2(b, v = 1)]k(O_2(b, v = 1); O_2)/\Psi_1}{[O_2(b, v = 0)]k(O_2(b, v = 0); CO_2)} - C_{v,N2}\frac{k(O_2(b, v = 0); N_2)}{k(O_2(b, v = 0); CO_2)} - C_{v,O2}\frac{k(O_2(b, v = 0); O_2)}{k(O_2(b, v = 0); CO_2)} - \frac{1}{N_t\tau_{O2(b,0)}k(O_2(b, v = 0); CO_2)} - C_{v,O3}\frac{k(O_2(b, v = 0); O_3)}{k(O_2(b, v = 0); CO_2)} \quad (7)$$

where N_t is the total atmospheric density at a given altitude, connected by the gas law with pressure and kinetic temperature. The reaction rate coefficients entering into the system of equations (3-6) are presented in Table 1.

Formula (7) reveals the relationship between the CO_2 concentration and the populations of $O_2(b^1\Sigma_g^-, v = 1)$ and $O_2(b^1\Sigma_g^-, v = 0)$. The denominators of all five terms in expression (7) include the rate coefficient $k(O_2(b, v=0);CO_2)$ of reaction $O_2(b^1\Sigma_g^-, v = 0) + CO_2 \rightarrow O_2(a^1\Delta_g, v = 0) + CO_2$, which was measured repeatedly from 1970 (see below).

Let us consider the experimental data on the rate coefficients of all reactions included in (7).

i) The rate coefficient $k(O_2(b, v=0);CO_2)$ has been measured since 1970 mainly at room temperature (Fig. 3a). Atkinson et al. (2004) described in details the initial period of measurements (up to 1990). Further studies were carried out in 1994 (Hohmann et al., 1994), in 2005 (Dunlea et al., 2005) and in 2017 (Zagidullin et al., 2017). All measurements, except for the data of (Wildt et al., 1988), give rather close values (Fig. 3a). There are only two attempts to measure the temperature dependence of $k(O_2(b, v=0);CO_2)$ (Fig. 3b). In the interval 245–362 K, no temperature dependence was observed in (Choo and Leu, 1985). A weak temperature dependence with a local minimum at 400 K is observed in (Zagidullin et al., 2017), but up to room temperature, the values $k(O_2(b, v=0);CO_2)$ are very close to the mean value for the data obtained for the period 1970–2017 within the experimental errors. Thus, there is no reason to doubt that $k(O_2(b, v=0);CO_2)$ is practically independent on temperature and equals to $(4.40 \pm 0.44)\cdot10^{-13}$ cm^3s^{-1} in the interval 245–362 K, where the error is estimated by the root-mean-square deviations for the entire data set.

ii) Currently value of the rate coefficient $k(O2(b, v = 0);O2)$ have been measured at room temperature and equal to $(4.1 \pm 2.0)\cdot10^{-17}$ cm^3s^{-1} (Atkinson et al., 2004) and/or $(3.0 \pm 0.6)\cdot10^{-17}$ cm^3s^{-1} (Zagidullin et al., 2017).

iii) The temperature dependence of $k(O2(b, v = 0);N2)$ has been investigated several times, starting from 1980 (Fig. 4). On the basis of careful analysis of the data of three experiments in which the temperature dependence was studied in the wide range of temperatures (Kohse-Hoinghaus and Stuhl, 1980; Choo and Leu, 1985; Zagidullin et al., 2017), we can conclude that $k(O2(b, v = 0);N2)$ does not depend on temperature in the range 210–370 K: $k(O2(b,v = 0);N2) = (2.20 \pm 0.24)\cdot10^{-15}$ cm^3s^{-1} (thick grey line in Fig. 4).

iv) $k(O2(b, v = 0);O3)$ was measured in (Atkinson et al., 2004; Sander et al., 2011) in the range of temperatures of 210–370 K with quite high accuracy (Table 1).

v) Measurements of the rate coefficient, $k(O_2(b, v=1);O_2)$, of the

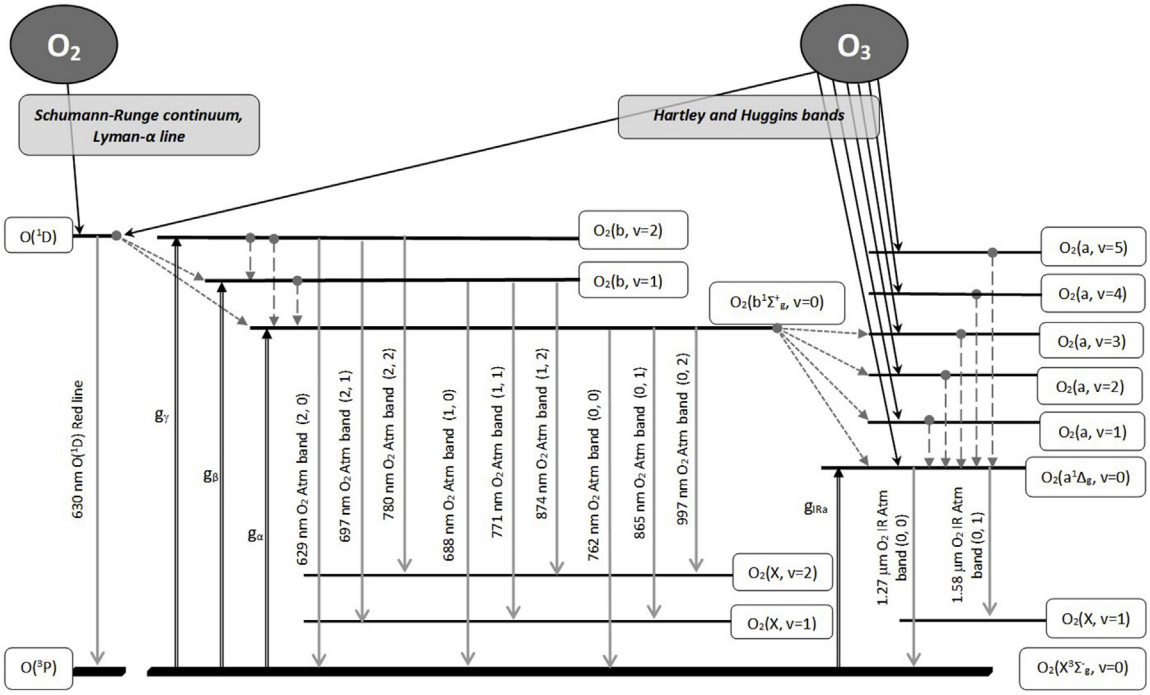

Fig. 1. The scheme of electronic-vibrational kinetics of the products of O_2 and O_3 photolysis in the MLT region (YM2011 model), taking into account 9 excited levels of the oxygen molecule (three levels $O_2(b^1\Sigma_g^+$, v = 0,1, 2), six levels $O_2(a^1\Delta_g$, v = 0–5)) and, also, the excited level of the oxygen atom, $O(^1D)$. Solid inclined lines with downwards arrows designate the processes of O_2 and O_3 photolysis. Double vertical lines with the arrows pointed upwards designate the processes of solar radiation resonance absorption in the 762 nm (g_α), 688 nm (g_β), 629 nm (g_γ) and in the 1.27 μm (g_{IRa}) bands. Short dashed black inclined lines with arrows present energy transfer from $O(^1D)$ to the $O_2(b^1\Sigma_g^+$, v = 0, 1) and from $O_2(b^1\Sigma_g^+$, v = 0) to $O_2(a^1\Delta_g$, v = 0–3) at collisional quenching. Long dashed vertical lines with downward arrows indicate collision transitions V-V transitions. Solid grey vertical lines with arrows pointed down designate the processes of radiative emissions from electronical-vibrational levels of O_2 molecule and from excited atom $O(^1D)$.

reaction $O_2(b^1\Sigma_g^+$, v = 1) + $O_2 \rightarrow O_2(X^3\Sigma_g^-$, v = 1) + $O_2(b^1\Sigma_g^+$, v = 0) were carried out in the wide temperature range with high accuracy in (Hwang et al., 1999) for 125–295 K and in (Pejakovic et al., 2005) for 292–1000 K (Fig. 5). The measured values of $k(O_2(b, v=1); O_2)$ agree well with each other at room temperature (Fig. 5). However, the interpolation of these values - $k(O_2(b, v=1);O_2) = (2.2 \pm 0.8)\cdot10^{-11}\cdot(T/292)^{1.0 \pm 0.3} exp(-(115 \pm 105)/T)$ cm^3s^{-1}, suggested in (Pejakovic et al., 2005) for the entire temperature range, 125–1000 K, has the average relative uncertainty $\xi \approx 0.53$. The uncertainty of interpolation (marked with black dashed lines in Fig. 5) are almost three times more than the experimentally measured errors of this coefficient.

Note, that in accordance with formulas (A3, A5 and A6) from the Appendix 1, using only the same experimental data we can obtain the alternative interpolation, $k(O_2(b, v=1);O_2) = (2.37 \pm 0.31)\cdot10^{-11}(T/292)^{1.09 \pm 0.09} exp(-(120 \pm 16)/T)$ cm^3s^{-1}. For this interpolation the mean value of relative uncertainty $\xi \approx 0.15$ for the entire temperature zone agrees with the limits of the experimental error bars (grey solid and dotted lines in Fig. 5). Finally, in order to avoid the further discussion about the interpolations of the values in the temperature interval 125–1000 K, for this work we used only the values of $k(O_2(b, v=1);O_2) = 4.2\cdot10^{-11} exp(-312/T)$ cm^3s^{-1}, measured by Hwang et al. (1999) for the temperatures that are typical for the MLT conditions, T = 125–295 K (Table 1 and unfilled squares in Fig. 5).

6. Analysis of the complete formulas for retrieving the altitude dependences of the CO_2 and O_3 volume mixing ratios in the mesosphere

In formula (7), the volume mixing ratios of O_2, $C_{v,O2}$, and N_2, $C_{v,N2}$, do not depend on altitude therefore we regard them as invariants. In addition, some parameters of the model, which do not depend on the gas temperature, are invariants, namely: $k(O_2(b, v=0);CO_2)$, $k(O_2(b, v=0);N_2)$, $k(O_2(b, v=0);O_2)$, Ψ_1 and $\tau_{O2(b, v)}$, as was shown above. The values of $C_{v,CO2}$, $C_{v,O3}$, $[O_2(b^1\Sigma_g^+, v=0)]$, $[O_2(b^1\Sigma_g^+, v=1)]$, g_α, g_β, T depend on the altitude.

In this case we rewrite (7), revealing the invariants explicitly:

$$C_{v,CO2} = \Omega_1 C_{v,O2}\frac{[O_2(b, v=1)]\omega_2 k(O_2(b, v=1); O_2) + g_\alpha + \omega_1 g_\beta}{[O_2(b, v=0)]} - \Omega_2 C_{v,O2} - \Omega_3 C_{v,N2} - \frac{\Omega_1\Omega_4 T}{p\tau_{O2(b,0)}} - \Omega_1 C_{v,O3} k(O_2(b, v=0); O_3) \quad (8)$$

where T – kinetic temperature in Kelvin and p – atmospheric pressure (mb) at a given altitude.

In Table 2 we present the values of invariants which can be easily estimated using Table 1.

The second term in (8), $\Omega_2 C_{v,O2}$, can be neglected, since this term is equal to $1.9\cdot10^{-5}$, which is two orders of magnitude smaller than the first term in (8). The third term is the invariant $\Omega_3 C_{v,N2}$, which is equal to $3.92\cdot10^{-3}$ and includes the rate coefficient of reaction of the main quenching process, $O_2(b^1\Sigma_g^+, v = 0) + N_2 \rightarrow products$ that provides up to 60–88% of the O_2 ($b^1\Sigma_g^+$, v = 0) total quenching factor in the mesosphere (Fig. 2d). The fourth term (inversely proportional to pressure) increases with the altitude and exceeds the value $1.3\cdot10^{-4}$ nearly 70 km. This term must be taken into account in determining $C_{v,CO2}$. The last term of (8) depends on the ozone concentration and, as shown in Sec. 3, becomes important below 60 km, where its value reaches $6\cdot10^{-5}$ and more.

The core of the proposed method for determining $C_{v,CO2}$ from measurements of the concentrations of the excited molecules $O_2(b^1\Sigma_g^+$, v = 1) and $O_2(b^1\Sigma_g^+$, v = 0) depending on altitude expresses the first term of expression (8): at the excitation of the both levels the O_3 and O_2 photodissociation processes play a key role, but the population of $O_2(b^1\Sigma_g^+$, v = 1) does not depend on CO_2, in contrast to $O_2(b^1\Sigma_g^+$, v = 0).

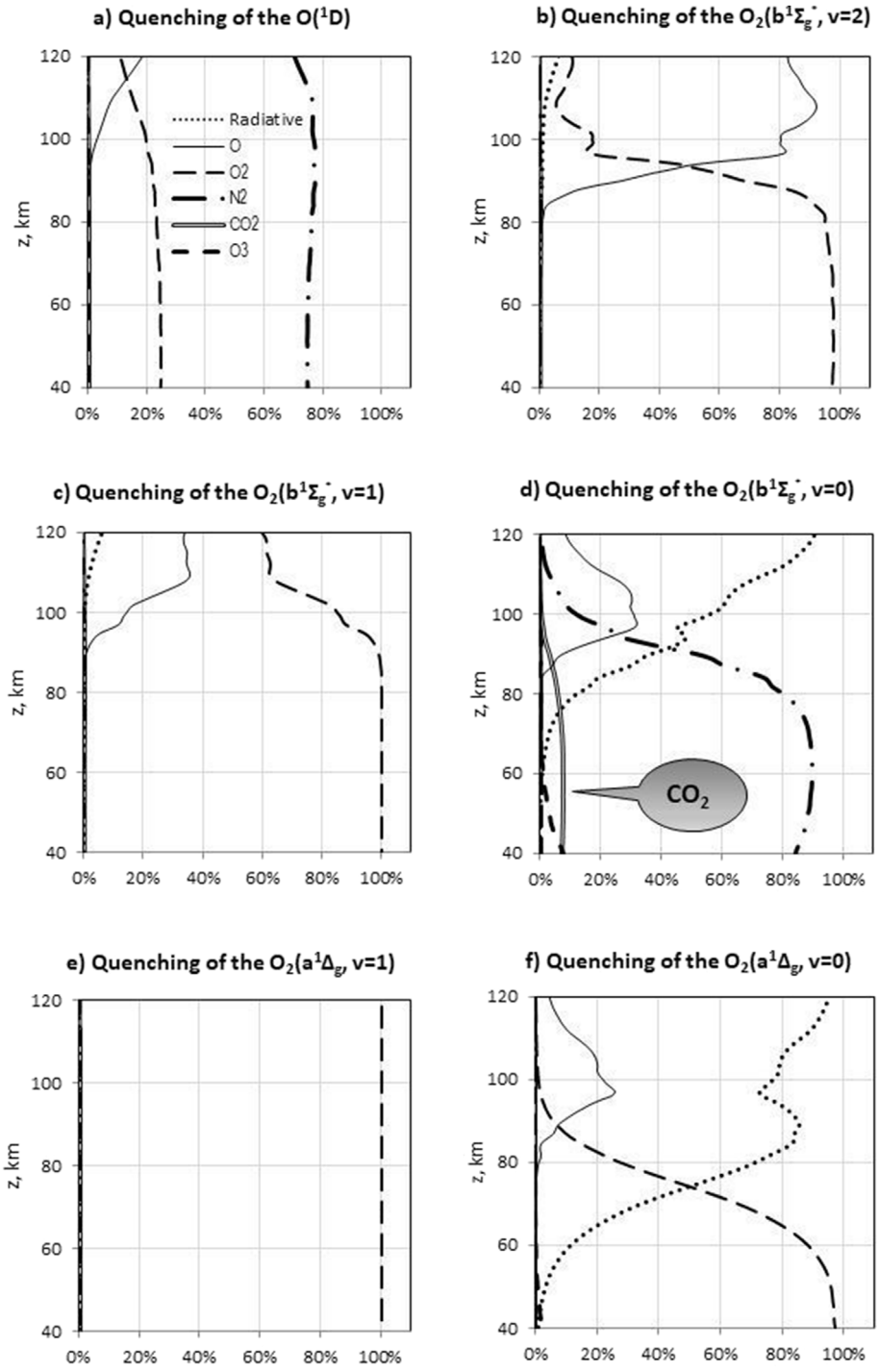

Fig. 2. The relative contributions of the radiative quenching and deexcitation processes in collisions with $O(^3P)$, O_2, N_2, CO_2 and O_3 to the quenching factors of $O(^1D)$, $O_2(b^1\Sigma_g^+, v = 2 - 0)$, $O_2(a^1\Delta_g, v = 0–1)$ for the typical SABER event, SABER L2, 2010, day 172, latitude 43.0, SZA = 70.5, F10.7 = 74. Different types of quenching are denoted by follows: dotted line – radiative processes; quenching in collisions with various atmospheric components: solid thin line – with $O(^3P)$, long dashed line – with O_2, dashed-dotted line – with N_2, double line – with CO_2, short dashed line – with O_3.

To determine these concentrations, it is necessary to measure the absolute values of the volume emission rate (*VER*) in the O_2 Atmospheric bands produced by transitions from the levels $O_2(b^1\Sigma_g^+, v = 0$ and 1).

$$VER(O_2(b^1\Sigma_g^+, v') \rightarrow O_2(X^3\Sigma_g^-, v'')) = [O_2(b^1\Sigma_g^+, v')] \cdot A(O_2\ Atm\ band\ (v', v'')) \quad (9)$$

In (9) $A(O_2\ Atm\ band\ (v', v''))$ is the Einstein coefficient of the corresponding transition from the level $O_2(b^1\Sigma_g^+, v')$ to $O_2(X^3\Sigma^-_g, v'')$ in the system of the O_2 Atmospheric bands (v', v") (Table 3).

The Einstein coefficients for these transitions and characteristic VER for radiance formed by transitions from $O_2(b^1\Sigma_g^+, v = 0)$ and $O_2(b^1\Sigma_g^+, v = 1)$ are presented in Table 7.1 and Fig. 15 of (Yankovsky et al., 2016).

Yee et al. (2012) give an overview of the episodic rocket measurements of the vertical profiles of VERs from $O_2(b^1\Sigma_g^+, v = 0)$ and $O_2(b^1\Sigma_g^+, v = 1)$. We have calculated VERs for 150 SABER events (22nd September 2010) for the latitude interval −44° to 75° (Yankovsky

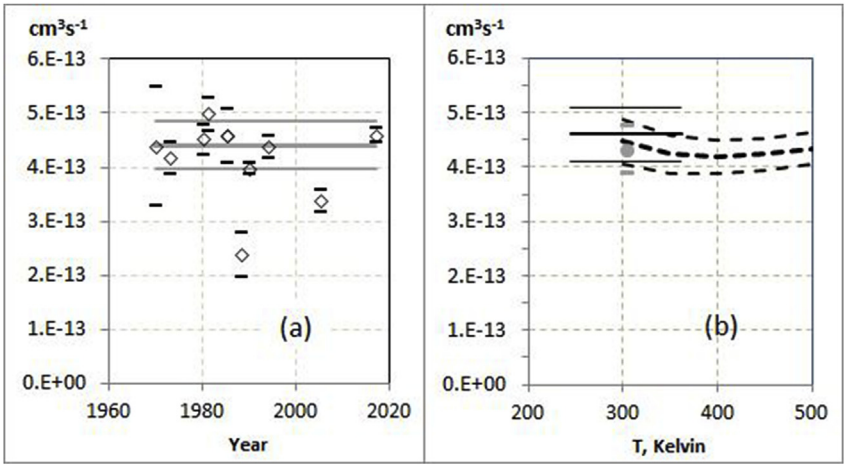

Fig. 3. (a) Unfilled diamonds – the measured at room temperature values of the rate coefficient of reaction $O_2(b^1\Sigma_g^+, v=0) + CO_2 \rightarrow products$, $k(O_2(b, v=0);CO_2)$, with error bars (during 1970–2017, see Section 5). Thick grey line with thin dashed bars – trend of $k(O_2(b, v=0);CO_2)$ values for these years. (b) The measured dependences of $k(O_2(b, v=0);CO_2)$ on temperature: thick line (Choo and Leu, 1985) at 245–362 K, thick dashed line (Zagidullin et al., 2017) at 300–800 K. Thin solid and dashed lines denote the standard deviation. Filled circle with error bars denotes the mean value of $k(O_2(b, v=0);CO_2)$ from Fig. 3(a) at room temperature.

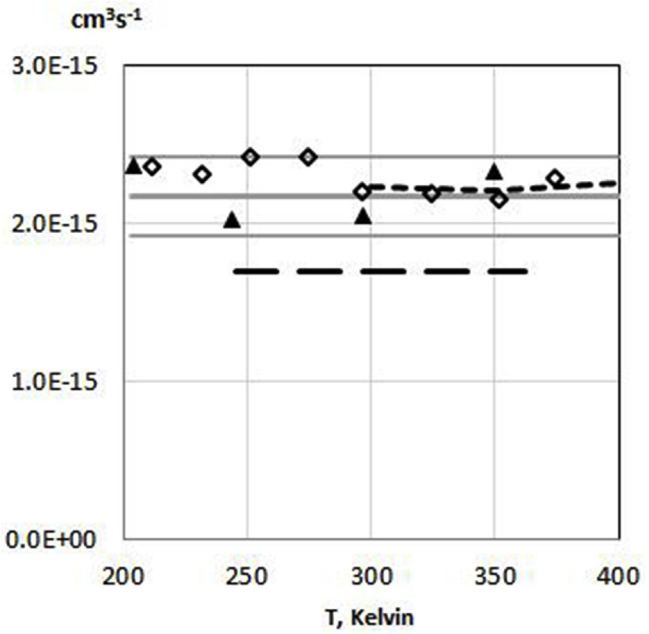

Fig. 4. The rate coefficient of reaction $O_2(b^1\Sigma_g^+, v = 0) + N_2 \rightarrow products$. Unfilled diamonds – from (Dunlea et al., 2005) at 210–373 K; filled triangles – (Kohse-Hoinghaus and Stuhl, 1980) at 203–349 K; long dashed line – (Choo and Leu, 1985) at 245–362 K; short dashed line – (Zagidullin et al., 2017) at 300–800 K. Thick grey line is the value of the reaction rate coefficient averaged over the experimental data (Dunlea et al., 2005; Kohse-Hoinghaus and Stuhl, 1980; Zagidullin et al., 2017) and the thin grey lines denote the standard deviation.

et al., 2016). In the altitude range 50–100 km the calculated VERs from $O_2(b^1\Sigma_g^+, v = 0)$ lie in the range $2{\cdot}10^4$ to $2{\cdot}10^5$ cm^{-3}s^{-1} and the experimental data (Yee et al., 2012) are in the range $4{\cdot}10^4$ to $1.5{\cdot}10^5$ cm^{-3}s^{-1}. The calculated VERs for the emission from $O_2(b^1\Sigma_g^+, v = 1)$ are in the interval $2{\cdot}10^1$ to $8{\cdot}10^2$ cm^{-3}s^{-1} and the experimental data are in the range of $1{\cdot}10^1$ to $1{\cdot}10^3$ cm^{-3}s^{-1}. For the VERs from $O_2(b^1\Sigma_g^+, v = 2)$ the data calculated by us are in the range from 0.1 to 3.0 cm^{-3}s^{-1}. Thus, in the altitude range 50–100 km the experimental values of VERs (Yee et al., 2012) lie in the range of the calculated VERs given in (Yankovsky et al., 2016).

Below 60 km, the role of quenching the $O_2(b^1\Sigma_g^+, v = 0)$ by ozone begins to increase (see section 3 and Fig. 2d) and one should take into account the last term of (8) (namely, $\Omega_5 C_{v,O3} k(O_2(b, v=0);O_3)$). In the framework of the YM2011 model we can estimate simultaneously the ozone volume mixing ratio by measuring the VER of the radiance formed by transition from the level $O_2(b^1\Sigma_g^+, v = 1)$. The sensitivity study performed in (Yankovsky et al., 2016) shows that $O_2(b^1\Sigma_g^+, v = 1)$ is the best proxy for the $[O_3]$ retrieval in the MLT region. From equations (3) and (5) we obtain an expression for the relative ozone content in this altitude interval from 50 to 85 km:

$$C_{v,O3} = \frac{C_{v,O2}}{J_{HHb} F(O_3 \rightarrow O(^1D); HHb)} \{\Omega_5 \omega_2([O_2(b, v = 1)] k(O_2(b, v = 1); O_2) - g_\beta) - J_{Ly\alpha} F(O_2 \rightarrow O(^1D); Ly\alpha)\} \quad (10)$$

Parameter Ω_5 included in (10)

$$\Omega_5 = 1 + \frac{C_{v,N2} k(O(^1D); N_2)}{C_{v,O2} k(O(^1D); O_2)} \quad (11)$$

depends on the ratio of the rate coefficients of reactions $O(^1D) + N_2 \rightarrow O + N_2^{\#}$ and $O(^1D) + O_2 \rightarrow O + O_2(b^1\Sigma_g^+, v)$. The rate coefficients of both reactions were measured with high accuracy (values of errors are nearly 9% (Yankovsky et al., 2016)), and their ratio is weakly temperature dependent (proportional to *exp*(31/T). In the temperature range typical for the mesosphere, parameter Ω_5 is equal to 4.10 ± 0.08 and is included in the table of invariants (see Table 2).

Thus, in accordance with (10), the uncertainty of the ozone mixing ratio $C_{v,O3}$ retrieval mainly depends not on the errors of the rate coefficients of these reactions, but on the following parameters: on the accuracy of measurements of *VER* ($O_2(b^1\Sigma_g^+, v = 1)$), and also on the rate coefficient of reaction $O_2(b^1\sum_g^+, v=1) + O_2 \rightarrow O_2(X^3\sum_g^-, v= 1) + O_2(O_2(b^1\sum_g^+, v= 0), k(O_2(b, v = 1), O_2)$. Another simplification of formula (10) for the ozone concentration retrieval is also possible: below 70 km, the photolysis of O_2 in the line H Lyman α can be neglected.

7. Analysis of the new method of the CO_2 volume mixing ratio retrieval in the mesosphere

7.1. The formula for the CO_2 volume mixing ratio retrieval in the mesosphere: application for remote sensing

Taking into account the analysis of formula for $C_{v,CO2}$ retrieval (8) performed in Section 6, we succeeded in obtaining the simple formula (12) for determining the volume mixing ratio CO_2 in the mesosphere which can be used for remote sensing from satellites:

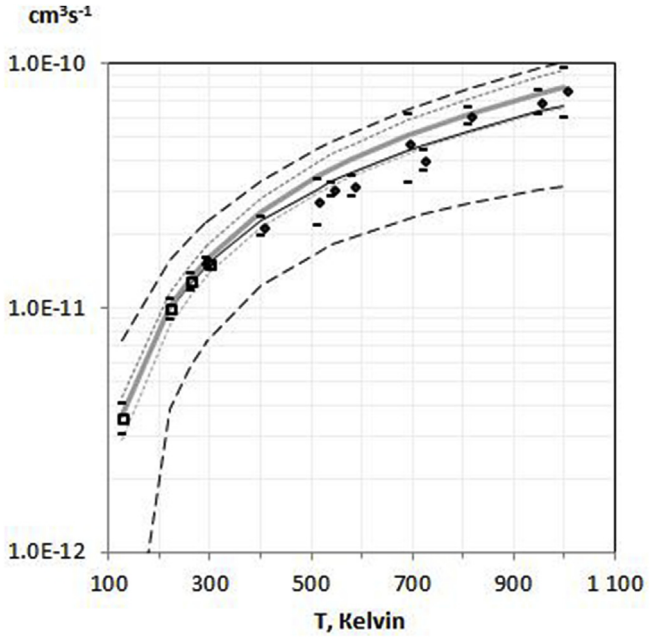

Fig. 5. The rate coefficient, $k(O_2(b, v=1);O_2)$, with the experimental error bars for the reaction $O_2(b^1\Sigma_g^+, v = 1) + O_2 \rightarrow products$: filled diamond – (Pejakovic et al., 2005), unfilled squares – (Hwang et al., 1999). Solid line – interpolation of (Pejakovic et al., 2005), dashed lines – the error limits. Solid grey line and grey dotted lines show the interpolation and corresponding error limits obtained in this study that we discuss in the text (Section 5).

Table 2
The values of the invariants for the inverse problems in the mesosphere and lower thermosphere, ξ - relative uncertainty of the invariant.

Invariant		Value	ξ	Dimension
ω_1	$1-\frac{1}{\Psi_1}$	−0.25	0.625	1
ω_2	$\frac{1}{\Psi_1}$	1.25	0.125	1
Ω_1	$\frac{1}{k(O_2(b,v=0);CO_2)}$	$2.27\cdot10^{12}$	0.10	$cm^{-3}s$
Ω_2	$\frac{k(O_2(b,v=0);O_2)}{k(O_2(b,v=0);CO_2)}$	$9.3\cdot10^{-5}$	0.32	1
Ω_3	$\frac{k(O_2(b,v=0);N_2)}{k(O_2(b,v=0);CO_2)}$	$5.0\cdot10^{-3}$	0.15	1
Ω_4	$\frac{1}{7.24\cdot10^{18}}$	$1.38\cdot10^{-19}$	0.00	$mb\cdot cm^3\cdot K^{-1}$
Ω_5	$1+\frac{C_{v,N2}k(O(^1D);N_2)}{C_{v,O2}k(O(^1D);O_2)}$	4.10	0.02	1
Ω_6	$\frac{k(O_2(b,v=0);O(^3P))}{k(O_2(b,v=0);CO_2)}$	$1.82\cdot10^{-1}$	0.27	1

Table 3
The wavenumber centers of the O_2 Atmospheric bands, $O_2(b^1\Sigma_g^+, v' \rightarrow X^3\Sigma_g^-, v'')$.

O_2 Atm band (v', v")	$O_2(X^3\Sigma_g^-, v"=0)$	$O_2(X^3\Sigma_g^-, v"=1)$	$O_2(X^3\Sigma_g^-, v"=2)$
$O_2(b^1\Sigma_g^-, v'=0)$	762.1	864.7	996.8
$O_2(b^1\Sigma_g^-, v'=1)$	688.4	771.0	874.4
$O_2(b^1\Sigma_g^-, v'=2)$	628.8	697.0	780.4

$$C_{v,CO2} = \Omega_1 C_{v,O2}\frac{[O_2(b,v=1)]\omega_2 k(O_2(b,v=1);O_2)+g_\alpha}{[O_2(b,v=0)]} - \Omega_3 C_{v,N2} - \frac{\Omega_1\Omega_4 T}{p\tau_{O2(b,0)}} - \Omega_1 C_{v,O3}k(O_2(b,v=0);O_3) \quad (12)$$

The following parameters of (12) depend on the altitude: $[O_2(b^1\Sigma_g^-, v = 1)]$, $[O_2(b^1\Sigma_g^-, v = 0)]$, $C_{v,O3}$, g_α, $k(O_2(b, v=1)O_2)$, $k(O_2(b, v=0);O_3)$ and gas temperature, T. In comparison with (8) the total contribution of the discarded terms ($\omega_1 g_\beta$ and $\Omega_2 C_{v,O2}$) in (12) is less than (1.0–1.5) %. The expression (12) is valid in the altitude interval from 50 to 85 km.

7.2. Sensitivity study of the $C_{v,CO2}$ retrieval problem

The estimation of the error of the $C_{v,CO2}$ retrieval, depending on the uncertainties of the parameters included in (12), was carried out on the basis of the sensitivity analysis method developed in (Yankovsky et al., 2016). The basic definitions used in sensitivity analysis are presented in Appendix 1.

From expression (12) we can get the sensitivity coefficients of $C_{v,CO2}$ to the parameters depending on altitude in the analytical form:

$$S(C_{v,CO2};[O_2(b,v=1)]) = \frac{\Omega_1\omega_2 C_{v,O2}[O_2(b,v=1)]k(O_2(b,v=1);O_2)}{C_{v,CO2}[O_2(b,v=0)]} \quad (13)$$

$$S(C_{v,CO2};[O_2(b,v=0)]) = -\frac{\Omega_1 C_{v,O2}(\omega_2[O_2(b,v=1)]k(O_2(b,v=1);O_2)+g_\alpha)}{C_{v,CO2}[O_2(b,v=0)]} \quad (14)$$

$$S(C_{v,CO2};g_\alpha) = \frac{\Omega_1 C_{v,O2} g_\alpha}{C_{v,CO2}[O_2(b,v=0)]} \quad (15)$$

$$S(C_{v,CO2};T) = -\frac{\Omega_1\omega_2 C_{v,O2}[O_2(b,v=1)]k(O_2(b,v=1);O_2)}{C_{v,CO2}[O_2(b,v=0)]}\left(\frac{b_3}{T}\right) - \frac{\Omega_1\Omega_4 T}{p\tau_{O2(b,v=0)}C_{v,O2}} + \frac{\Omega_1 C_{v,O3}k(O_2(b,v=0);O_3)}{C_{v,CO2}}\left(\frac{b_4}{T}\right) \quad (16)$$

$$S(C_{v,CO2};C_{v,O3}) = -\frac{\Omega_1 C_{v,O3}k(O_2(b,v=0);O_3)}{C_{v,CO2}} \quad (17)$$

$$S(C_{v,CO2};k(O_2(b,v=0);O_3)) \equiv S(C_{v,CO2};C_{v,O3}) \quad (18)$$

$$S(C_{v,CO2};k(O_2(b,v=1);O_2)) \equiv S(C_{v,CO2};[O_2(b,v=1)]) \quad (19)$$

Where in (16): $b_3 = -312\,K$ for rate coefficient $k(O_2(b, v=1);O_2) = 4.2\cdot10^{-11}exp(b_3/T)$ cm^3s^{-1} and $b_4 = -135\,K$ for rate coefficient $k(O_2(b, v=0);O_3) = 3.5\cdot10^{-11}exp(b_4/T)$ cm^3s^{-1} (Table 1).

The sensitivity coefficients of the $C_{v,CO2}$ to parameters of (12) are shown in Fig. 6 as functions depending on altitude. There is a very low sensitivity of the $C_{v,CO2}$ to $C_{v,O3}$ and, accordingly, to the rate coefficient of the reaction $O_2(b^1\Sigma_g^-, v = 0) + O_3 \rightarrow 2O_2 + O(^3P)$, $k(O_2(b, v = 0);O_3)$ (see (18) and Fig. 6).

7.3. Uncertainty analysis of the $C_{v,CO2}$ retrieval problem

The relative uncertainty of the retrieved values of $C_{v,CO2}$ were estimated using the formula (A2) in the Appendix 1 and the sensitivity coefficients (13-19):

$$\frac{\Delta C_{v,CO2}}{C_{v,CO2}} = \sqrt{\left(\sum_{v=0}^{1}(S(C_{v,CO2};[O_2(b,v)])\cdot\xi_{O2(b,v)})^2 + (S(C_{v,CO2};T)\cdot\xi_T)^2 + \sum_i (S(C_{v,CO2};z_i)\cdot\xi_i)^2\right)} \quad (20)$$

We divided all parameters affecting the retrieval of $C_{v,CO2}$ in (12) in three groups: parameters included in the first term in the radicand - the populations of the levels $O_2(b^1\Sigma_g^-, v = 1)$ and $O_2(b^1\Sigma_g^-, v = 0)$ from which the $C_{v,CO2}$ is determined; in the second term – T, temperature of the gas, as an independently obtained parameter; in the third term – the predefined parameters z_i, $C_{v,O3}$, g_α and the rate coefficients of two reactions, $k(O_2(b, v=1);O_2)$ и $k(O_2(b, v=0);O_3)$.

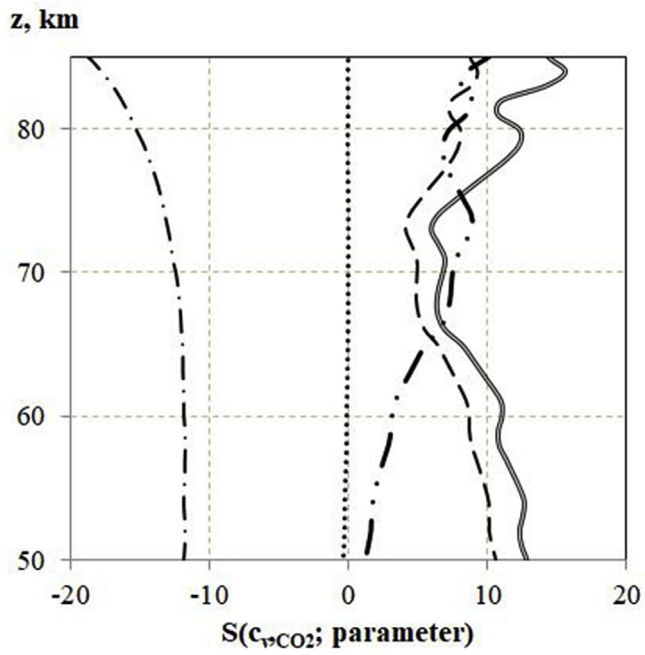

Fig. 6. The coefficients of sensitivity $C_{v,\ CO2}$ to the measured parameters $[O_2(b^1\Sigma_g^+, v = 1)]$ (dashed line), $[O_2(b^1\Sigma_g^+, v = 0)]$ (dashed-dotted line), and to other parameters of YM2011 model (T (solid double line), g_α (dashed-two dotted line), $C_{v,O3}$ (dotted line)). For calculations of $S(C_{v,\ CO2}$; parameter) we used the altitude profiles $[O_2]$, $[N_2]$, $[O_3]$, $[CO_2]$, T for the typical SABER event: SABER L2, 2010, day 172, latitude 43.0, SZA = 70.5, F10.7 = 74.

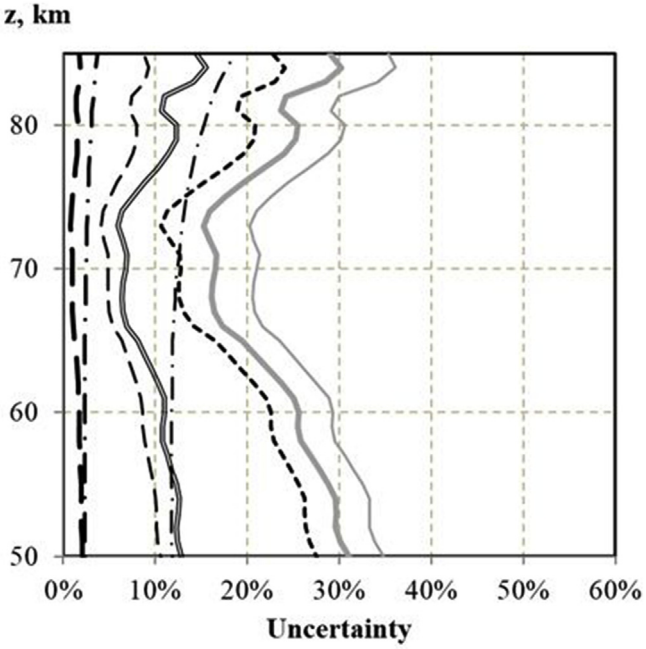

Fig. 7. The total relative uncertainty of the $C_{v,CO2}$ retrieval (thick grey line) and the contributions to it due to errors of the 'measured' $[O_2(b^1\Sigma_g^+, v = 1)]$ (thick long dashed line), and $[O_2(b^1\Sigma_g^+, v = 0)]$ (thick dashed-dotted line) with relative accuracy of measurements 0.002 (thick lines). The total relative uncertainty of the $C_{v,CO2}$ retrieval (thin grey line) and the contributions to it due to errors of the 'measured' $[O_2(b^1\Sigma_g^+, v = 1)]$ (thin long dashed line), and $[O_2(b^1\Sigma_g^+, v = 0)]$ (thin dashed-dotted line) with relative accuracy of measurements 0.01 (thin lines). The contributions of other parameters to the total uncertainty: short dashed line - uncertainty of $k(O2(b, v=1):O2)$ with value $\xi = 0.026$ (Hwang et al., 1999), double solid line – of gas temperature, T with uncertainty $\xi = 0.01$ (Rezac et al., 2015).

To demonstrate the influence of the key parameters we carried out the numerical experiment. The relative error in measuring the concentrations of $O_2(b^1\Sigma_g^+, v = 1)$ and $O_2(b^1\Sigma_g^+, v = 0)$ (or, equivalently, VER of the corresponding O_2 Atmospheric bands) was assumed to be either 0.2%, or 1.0%. For estimation of the total uncertainty of the $C_{v,CO2}$ retrieval we used the constant values of the relative uncertainties: $\xi_{Cv,O3} \approx 10\%$ (estimation on base (Smith et al., 2013)), $\xi_T \approx 1\%$ (Rezac et al., 2015), $\xi_{g\alpha} \approx 1\%$, $\xi_{k(O2(b,v=0);O3)} = 15\%$, $\xi_{k(O2(b,v=1);O2)} = 2.6\%$ (Hwang et al., 1999) and see Table 1.

The total relative uncertainty of the $C_{v,CO2}$ retrieval and also the individual contributions from different parameters of (20) are shown in Fig. 7.

As can be seen from (Fig. 7), the predefined parameters – the rate constant $k(O2(b, v=1);O2$ and the gas temperature, T, give the essential, but fixed contribution to the uncertainty of the $C_{v,CO2}$ retrieval, because the contributions of these parameters do not depend on accuracy of measured in experiment the $[O_2(b^1\Sigma_g^+, v = 0)]$ and $[O_2(b^1\Sigma_g^+, v = 1)]$. We carried out the numerical experiment to determine of the role of accuracy of the measurements of the O_2 Atmospheric bands intensities on the uncertainty of the $C_{v,CO2}$ retrieval. The expected uncertainty of the retrieved CO_2 mixing ratio altitude profile in the mesosphere can be within 15–30%, depending on the altitude, but the real accuracy of the $C_{v,CO2}$ retrieval may be better because the uncertainty analysis gives only estimation of the influence of different parameters on the total uncertainty. The numerical experiment demonstrated the essential role of the measurement's accuracy of the emission intensities in the O_2 Atmospheric bands (see the solid and dashed curves in Fig. 7).

8. Discussion

In this study we developed the two-channel method of simultaneously retrieving the concentration profiles of the two components O_3 and CO_2 in the altitude range of 50–85 km.

The method is realized using formulas (10) and (12), assuming simultaneous measurements of the VER of emissions from the levels $O_2(b^1\Sigma_g^+, v = 1)$ and $O_2(b^1\Sigma_g^+, v = 0)$ with relative accuracy of these measurements which is not worse than 0.2–1.0%. We cannot discuss the proposed new method for retrieving the $[CO_2]$ altitude profile in details up to its practical implementation. However, we can make some additional remarks.

8.1. Comparison of the new method of the [CO_2] profile retrieval with experimental data in the mesosphere

In the practical implementation of the proposed method for retrieving the $[CO_2]$ altitude profile one cannot exclude the incompleteness of modern data on the rate constants of certain reactions (the absence of data or systematic errors in determining the temperature dependence of the rate coefficients). Therefore, it is necessary to foresee the possibility of independent validation of the basic formula (12) for the $C_{v,CO2}$ retrieval. The two possible options for calibrating the applied formula (12) for $C_{v,CO2}$ retrieval are:

a) comparison of the altitude profile of $C_{v,CO2}$ retrieved from (12) with it measured in an experiment of the type ACE-FTP at sunset or sunrise;
b) integration of the $C_{v,CO2}$ values from (12) over the altitude and comparing the value of the integral with the measured total carbon dioxide content in the same altitude interval.

8.2. Proposal on the three-channel method of simultaneous retrieval of the concentration profiles of three components O(^{3}P), O_3 and CO_2 in the altitude range of 85–100 km

Let's discuss a possible approach to the problem of simultaneous retrieval of the concentration profiles of three components O(^{3}P), O_3 and CO_2 in the altitude range of 85–100 km (characteristic altitudes here and thereafter are given approximately, with a deviation of 2–3 km

in both sides, since the specific situation in the atmosphere depends on the latitude, season, etc.). The task is becoming more urgent due to the effect of increasing CO_2 at altitudes above 80 km for 10 years that discovered in recent years (Emmert et al., 2012; Garcia et al., 2014; Rezac et al., 2015; Yue et al., 2015; Qian et al., 2017). According to (Yue et al., 2015) the SABER and ACE-FTS $[CO_2]$ altitude profiles demonstrate a faster increase the $[CO_2]$ above 80 km for 10 years, compared to SD-WACCM model (Smith et al., 2011). The SABER CO_2 trend shows a peak at ~110 km of about 12% per decade.

The problem can be theoretically solved by using the individual proxy for each of the target component (Yankovsky et al., 2016). In this study and also in (Yankovsky et al., 2016), using a sensitivity study and uncertainty analysis of the model of kinetics of O_3 and O_2 photolysis in the MLT, YM2011, we have tested six excited components, namely, the electronically-vibrationally excited molecules $O_2(b^1\Sigma_g^+, v = 0, 1, 2)$ and $O_2(a^1\Delta_g, v = 0, 1)$, and also excited atom $O(^1D)$ as $O(^3P)$, CO_2 and O_3 proxies. In (Yankovsky, 2017) we have shown that, in principle, at using the emissions from three excited levels $O_2(b^1\Sigma_g^+, v = 0, 1, 2)$, the simultaneously retrievals of the $[O(^3P)]$, $[O_3]$ and $[CO_2]$ are possible in the altitude range of 85–100 km.

The key parameter in this altitude range is the atomic oxygen. As it shown in Fig. 2, the O (^3P) proxy can be any of the levels $O_2(b^1\Sigma_g^+, v = 0, 1$ or 2), and there cannot be $O_2(a^1\Delta_g, v)$, and also $O(^1D)$ levels, at least, below 120 km. The optimal proxy of $O(^3P)$ is $O_2(b^1\Sigma_g^+, v = 2)$ (see Fig. 2b and Sec. 5.4 in (Yankovsky et al., 2016)). According to the expression for the quenching factor of $O_2(b^1\Sigma_g^+, v = 2)$ (2), we estimated the total contribution of the three quenching channels of $O_2(b^1\Sigma_g^+, v = 2)$ (in collisions with O_3, N_2, CO_2), which turned out to be less than 0.5%, as can be seen from Fig. 2b. Among the processes of deactivation of $O_2(b^1\Sigma_g^+, v = 2)$, collisions with atomic and molecular oxygen as well as radiation quenching prevail.

Therefore, from the balance equation (4) and the quenching factor (2), we obtain a simple formula for retrieving the altitude profile of the VMR of atomic oxygen from $[O_2(b^1\Sigma_g^+, v = 2)]$ at altitudes above 85 km:

$$C_{v,O(3P)} = \frac{1}{k(O_2(b, v = 2); O(^3P))}\left\{C_{v,O2}\left(\frac{g_\gamma}{[O_2(b, v = 2)]} - k(O_2(b, v = 2); O_2)\right) - \frac{\Omega_4 T}{p\tau_{O2(b,2)}}\right\} \quad (21)$$

The radiative quenching of $O_2(b^1\Sigma_g^+, v = 2)$ (the last term in (21)) begins to affect approximately at 100 km and above (see Fig. 2b).

Taking into account $C_{v,O(3P)}$, from (21) and also expressions (2, 3, 6) we obtain the formula for retrieving the altitude profile of the volume mixing ratio, $C_{v,CO2}$, in the interval 85–100 km:

$$C_{v,CO2} = \Omega_1 C_{v,O2}\frac{[O_2(b, v = 1)]\omega_2(k(O_2(b, v = 1); O_2) + C_{v,O(3P)}k(O_2(b, v = 1); O(^3P))/C_{v,O2}) + g_\alpha}{[O_2(b, v = 0)]} - \Omega_3 C_{v,N2} - \frac{\Omega_1\Omega_4 T}{p\tau_{O2(b,0)}} - \Omega_1 C_{v,O3}k(O_2(b, v = 0); O_3) - \Omega_6 C_{v,O(3P)} \quad (22)$$

The expression for retrieving the altitude profile $C_{v,O3}$ in the altitude range 85–100 km, derived from (5) and (2), also depends on the $C_{v,O(3P)}$ (21):

$$C_{v,O3} = \frac{C_{v,O2}}{J_{HHb}F(O_3 \rightarrow O(^1D); HHb)}\{\Omega_5\omega_2([O_2(b, v = 1)](k(O_2(b, v = 1); O_2) + k(O_2(b, v = 1); O(^3P))C_{v,O(3P)}/C_{v,O2}) - g_\beta) - (J_{SRC} + J_{Ly\alpha}F(O_2 \rightarrow O(^1D); Ly\alpha))\} \quad (23)$$

In (21-23) we used the invariants from Table 2. The estimation of accuracy of simultaneous retrieval of the concentration profiles of three components $O(^3P)$, O_3 and CO_2 (equations 21-23) in the altitude range of 85–100 km could be considered after the method of $C_{v,CO2}$ retrieval is practically realized for altitudes of 50–85 km.

9. Conclusions

9.1 We have formulated the multi-channel method for retrieval of the $[O(^3P)]$, $[O_3]$ and $[CO_2]$ altitude profiles in the daytime mesosphere and lower thermosphere from the simultaneous measurements of intensities (VER) of three emissions formed by transitions from the three electronically-vibrationally excited states, $O_2(b^1\Sigma_g^+, v = 2)$, $O_2(b^1\Sigma_g^+, v = 1)$ and $O_2(b^1\Sigma_g^+, v = 0)$. All these states of O_2 are excited in result of photodissociation of O_2 and O_3 and also at resonance absorption of solar radiation. Besides of that, the populations of these states depend on the O_3, O (^3P), O_2, N_2 and CO_2, concentration distributions in the MLT region. Only using the YM2011 model allowed us to consider in detail the complex groups of the processes of excitation and quenching of the states $O_2(b^1\Sigma_g^+, v = 0, 1, 2)$, the transitions from which form the system of the O_2 Atmospheric bands observed in the dayglow of the Earth. An important feature of the multi-channel method is that it can be used throughout the day and does not require the solution of complex problems of radiation transfer in the case of LTE breaking.

9.2 In the framework of the photochemical model YM2011, for the first time, we developed in details the two-channel method of simultaneously retrieval of the volume mixing ratios of O_3 and CO_2 in the altitude range 50–85 km (sections 6 and 7, see also Table 4). The method of the $C_{v,O3}$ retrieval in the altitude range 50–85 km is based on measurements of emission from the level $O_2(b^1\Sigma_g^+, v = 1)$ in 771.0, 874.4 or 688.4 nm bands and of the $C_{v,CO2}$ retrieval on measurements of emission from the level $O_2(b^1\Sigma_g^+, v = 0)$ in 762.1 or 864.7 nm bands. The core of the proposed method for determining $C_{v,CO2}$ from measurements of the concentrations of excited specious $O_2(b^1\Sigma_g^+, v = 1)$ and $O_2(b^1\Sigma_g^+, v = 0)$ depending on the altitude is based on the following: at excitation of both levels, the processes of O_3 and O_2 photodissociation play a key role, but the population of $O_2(b^1\Sigma_g^+, v = 1)$ does not depend on the $[CO_2]$, in contrast to $O_2(b^1\Sigma_g^+, v = 0)$. The obtained formulas (10, 12) can be used for remote sensing of the $C_{v,O3}$ and $C_{v,CO2}$ in the Earth atmosphere from satellites. Using the sensitivity study we have analyzed the expected uncertainties of the retrieved $C_{v,}$,$_{CO2}$ values.

9.3 In principle, multi-channel method allows us to retrieve simultaneously the three components $[O(^3P)]$, $[O_3]$ and $[CO_2]$ in the interval 85–100 km at using the measurements of intensities of the three emissions formed by transitions from three different levels $O_2(b^1\Sigma_g^+, v = 0, 1$ and 2). For the first time we present the formulas (20, 21 and 22) for the $C_{v,O3}$, $C_{v,CO2}$ and $C_{v,O(3P)}$ altitude profiles retrieval.

9.4 The two-channel and three-channel methods allows us to retrieve simultaneously altitude distributions of the volume mixing ratios of O_3 and CO_2 in the range 50–100 km and volume mixing ratio of O (^3P) above 85 km in the daytime MLT. Thus, the developed methods create the basis for calculating the altitude-latitude-longitude distributions of the volume mixing ratios of O_3, $O(^3P)$ and CO_2 in the calm daytime mesosphere and lower thermosphere.

9.5 It can be noted, that above 100 km–140 km, the $[O(^3P)]$ profile can be obtained using the measured VER in the O_2 Atmospheric bands

Table 4
Proxies, altitude ranges and O_2 emission bands for $[O(^3P)]$, $[O_3]$ and $[CO_2]$ retrieval.

Proxy	Altitude range for retrieval, km			Center of emission bands of proxies, nm
	$[O(^3P)]$	$[O_3]$	$[CO_2]$	
$O_2(b^1\Sigma_g^+, v = 2)$	85–140	no	no	628.8 or 697.0
$O_2(b^1\Sigma_g^+, v = 1)$	115–140	50–100	no	771.0 or 688.4
$O_2(b^1\Sigma_g^+, v = 0)$	105–130	80–100	50–100	762.1 or 864.7

formed by transitions from any excited levels $O_2(b^1\Sigma_g^+$, v = 0, 1 or 2). We examined this problem in detail on the basis of the sensitivity study and uncertainty analysis earlier in (Yankovsky et al., 2016).

9.6 As a summary, we present in the Table 4 the proxies for the [$O(^3P)$], [O_3] and [CO_2] retrieval, the altitude ranges in which the developed methods of retrieval can be used, as well as the centers of the O_2 Atmospheric bands that form the emissions corresponding to each proxy.

Author contributions

The author Yankovsky V. A. expressed the idea of the method and derived the basic formulas, the author Manuilova R. O. detailed the content of the paper and compared this method with alternative approaches. Concept, design, and manuscript preparation were joint efforts of both authors.

Conflicts of interest

No competing interests are present.

Acknowledgments

Funding: This work was supported by the Russian Foundation for Basic Research (grant RFBR No.17-05-00532). We thank three anonymous referees for their valuable suggestions to improve the present study.

Appendix 1

About on analytical approach in sensitivity and uncertainty studies

If the target function x_m depend on the n_z parameters z_i then the sensitivity coefficient of the target function to variation of parameter z_i, $S(x_m; z_i)$, is:

$$S(x_m; z_i) = \frac{z_i}{x_m} \cdot \frac{\partial x_m}{\partial z_i} \tag{A1}$$

The relative uncertainty of xm is connected with the sensitivity coefficients, and also with the relative errors of all parameters included, ξ_i (formula (12) in Yankovsky et al. (2016)):

$$\frac{\Delta x_m}{x_m} = \sqrt{\sum_{i=1}^{n_z} (S(x_m; z_i))^2 \cdot (\xi_i)^2} \tag{A2}$$

We use the experimentally determined values of the relative errors of the parameters $\xi_i = \Delta z_i / z_i$. The values of rate coefficients and quantum yields, as well as the values of their absolute uncertainties, have been obtained from available experimental data (see Table 1).

It is possible to carry out a sensitivity study to all parameters included in the balance equation system (1), namely: the concentration of excited molecules of $O_2(b^1\Sigma_g^+$, v = 0–2), $O_2(a^1\Delta_g$, v = 0–5) and the atom $O(^1D)$ (in cm^{-3}); the parameters of the model YM2011, z_i, (e.g., the main atmospheric component concentrations, the rates of photoexcitation processes, the quantum yields of the reaction products, the rate coefficients of quenching reaction of the component x_m in the radiative and collisional processes and so forth).

Example of analytical description of rate coefficient uncertainty using formulas (A1) and (A2)

The interpolation of the values of the reaction rate coefficient in the generalized Arrhenius form depends on three parameters A, b, n, each of which can have an individual uncertainty:

$$k(T) = (A \pm \Delta A)\left(\frac{T}{292}\right)^{n \pm \Delta n} exp\left(\frac{b \pm \Delta b}{T}\right) \tag{A3}$$

The total uncertainty of the values of k(T) can be calculated in the framework of the sensitivity study (see formula (A2)):

$$\frac{\Delta k}{k} = \sqrt{\left(S(k; A)^2\left(\frac{\Delta A}{A}\right)^2 + S(k; n)^2\left(\frac{\Delta n}{n}\right)^2 + S(k; b)^2\left(\frac{\Delta b}{b}\right)^2\right)} \tag{A4}$$

where the sensitivity coefficients of target function *k(T)* for the corresponding parameters from (A1):

$$S(k; A) = 1$$

$$S(k; n) = n \cdot ln\left(\frac{T}{292}\right) \tag{A5}$$

$$S(k; b) = \frac{b}{T}$$

Thus, the expression for the relative uncertainty of the values of *k(T)* from (A4) for the generalized Arrhenius form also depends on the temperature:

$$\frac{\Delta k}{k} = \sqrt{\left(\left(\frac{\Delta A}{A}\right)^2 + \left(\Delta n \cdot ln\left(\frac{T}{292}\right)\right)^2 + \left(\frac{\Delta b}{T}\right)^2\right)} \tag{A6}$$

It is also possible to solve the “inverse problem” using (A3 and A6). If in the experiment a number of measurements of the values of reaction rate coefficients (with a certain statistical errors) are obtained at different temperatures, then Arrhenius parameters, *A*, *b*, *n*, can be determined together with their uncertainties.

References

Atkinson, R., Baulch, D.L., Cox, R.A., Crowley, J.N., Hampson, R.F., Hynes, R.G., Jenkin, M.E., Rossi, M.J., Troe, J., 2004. Evaluated kinetic and photochemical data for atmospheric chemistry: volume I – gas phase reactions of Ox, HOx, NOx and SOx species. Atmos. Chem. Phys. 4, 1461–1738. http://dx.doi.org/10.5194/acp-4-1461-2004.

Beagley, S.R., Boone, C.D., Fomichev, V.I., Jin, J.J., Semeniuk, K., McConnell, J.C., Bernath, P.F., 2010. First multi-year occultation observations of CO_2 in the MLT by ACE satellite: observations and analysis using the extended CMAM. Atmos. Chem. Phys. 10, 1133–1153. http://dx.doi.org/10.5194/acp-10-1133-2010.

Brasseur, G.P., Solomon, S.C., 2005. Aeronomy of the Middle Atmosphere, third ed. Springer, Dordrecht 644 pages.

Choo, K.Y., Leu, M.T., 1985. Rate coefficients for the quenching of metastable $O_2(b^1\Sigma_g^+)$ molecules. Int. J. Chem. Kinet. 17, 1159–1167.

Dunlea, E.J., Talukdar, R.K., Ravishankara, A.R., 2005. Kinetics studies of the reactions of $O_2(b^1\Sigma_g^+)$ with several atmospheric molecules. J. Phys. Chem. 109A, 3912–3920.

Emmert, J.T., Stevens, M.H., Bernath, P.F., Drob, D.P., Boone, C.D., 2012. Observations of increasing carbon dioxide concentration in Earth's thermosphere. Nature Geoscience, Letter 5, 868–871. http://dx.doi.org/10.1038/ngeo1626.

Feofilov, A.G., Kutepov, A.A., 2012. Infrared Radiation in the Mesosphere and Lower Thermosphere: Energetic Effects and Remote Sensing Surveys in Geophysics, vol. 33. pp. 1231–1280. http://dx.doi.org/10.1007/s10712-012-9204-0.

Garcia, R.R., López-Puertas, M., Funke, B., Marsh, D.R., Kinnison, D.E., Smith, A.K., González-Galindo, F., 2014. On the distribution of CO_2 and CO in the mesosphere and lower thermosphere. J. Geophys. Res. Atmos. 119, 5700–5718. http://dx.doi.org/10.1002/2013JD021208.

Hohmann, J., Müller, G., Schonnenbeck, G., Stuhl, F., 1994. Temperature-dependent quenching of $O_2(b^1\Sigma_g^+)$ by H_2, D_2, CO_2, HN_3, DN_3, HNCO and DNCO. Chem. Phys. Lett. 217, 577–581.

Hwang, E.S., Bergman, A., Copeland, R.A., Slanger, T.G., 1999. Temperature dependence of the collisional removal of $O_2(b^1\Sigma_g^+$, v = 1 and 2) at 110-260 K, and atmospheric applications. J. Chem. Phys. 110, 18–24.

Jurado-Navarro, Á.A., López-Puertas, M., Funke, B., García-Comas, M., Gardini, A., González-Galindo, F., Stiller, G.P., von Clarmann, T., Grabowski, U., Linden, A., 2016. Global distributions of CO_2 volume mixing ratio in the middle and upper atmosphere from MIPAS high resolution spectra. Atmos. Meas. Tech. Discuss. http://dx.doi.org/10.5194/amt-2016-63.

Kaufmann, M., Gusev, O., Grossmann, K.U., Roble, R.G., Hagan, M.E., Hartsough, C., Kutepov, A., 2002. The vertical and horizontal distribution of CO2 densities in the upper mesosphere and lower thermosphere as measured by CRISTA. J. Geophys. Research D 107, 8182–8201.

Kohse-Hoinghaus, K., Stuhl, F., 1980. H2-laser photochemical study of the temperature dependent quenching of $O_2(b^1\Sigma_g^-)$. J. Chem. Phys. 72, 3720–3726.

Krupenie, P.H., 1972. The spectrum of molecular oxygen. J. Phys. Chem. Ref. Data 1, 423–521.

López-Puertas, M., Taylor, F.W., 2001. Non-lte Radiative Transfer in the Atmosphere. World Scientific Pub., Singapore 487 pages.

Martyshenko, K., Yankovsky, V., 2017. IR band of O_2 at 1.27 μm as the tracer of O_3 in the mesosphere and lower thermosphere: correction of the method. Geomagn. Aeron. 57, 229–241. http://dx.doi.org/10.1134/S0016793217020098.

Mlynczak, M.G., Marshall, B.T., Martin-Torres, F., Russell III, J.M., Thompson, R.E., Remsberg, E.E., Gordley, L.L., 2007. Sounding of the Atmosphere using Broadband Emission Radiometry observations of daytime mesospheric $O_2(a^1\Delta_g)$ 1.27 μm emission and derivation of ozone, atomic oxygen, and solar and chemical energy deposition rates. J. Geophys. Research D 112http://dx.doi.org/10.1029/2006JD008355. D15306.

Mlynczak, M.G., Solomon, S.C., Zaras, D.S., 1993. An updated model for $O_2(a^1\Delta_g)$ concentrations in the mesosphere and lower mesosphere and implications for remote sensing of ozone at 1.27 μm. J. Geophys. Res. 98D, 18639–18648.

Newman, S.M., Orr-Ewing, A.J., Newnham, D.A., Ballard, J., 2000. Temperature and pressure dependence of line widths and integrated absorption intensities of the $O_2(a^1\Delta_g - X^3\Sigma_g^-$ (0, 0)). J. Phys. Chem. 104A (42), 9467–9480.

Pejakovic, D.A., Wouters, E.R., Phillips, K.E., Slanger, T.G., Copeland, R.A., Kalogerakis, K.S., 2005. Collisional removal of $O_2(b^1\Sigma_g^+$, v = 1) by O_2 at thermospheric temperatures. J. Geophys. Research A 110A, 10. http://dx.doi.org/10.1029/2004JA010860. A03308.

Qian, L., Burns, A.G., Solomon, S.C., Wang, W., 2017. Carbon dioxide trends in the mesosphere and lower thermosphere. J. Geophys. Res. Space Physics 122, 4474–4488. http://dx.doi.org/10.1002/2016JA023825.

Rezac, L., Kutepov, A., Russell III, J.M., Feofilov, A.G., Yue, J., Goldberg, R.A., 2015. Simultaneous retrieval of T(p) and CO_2 VMR from two-channel non-LTE limb radiances and application to daytime SABER/TIMED measurements. J. Atmos. Sol. Terr. Phys. 130–131, 23–42. http://dx.doi.org/10.1016/j.jastp.2015.05.004.

Sander, S.P., Friedl, R.R., Abbatt, J.P.D., Barker, J.R., Burkholder, J.B., Golden, D.M., Kolb, C.E., Kurylo, M.J., Moortgat, G.K., Wine, P.H., Huie, R.E., Orkin, V.L., 2011. Chemical Kinetics and Photochemical Data for Use in Atmospheric Studies. JPL Publication 10–16, Evaluation Number 17. California Institute of Technology, Pasadena, California.

Smith, A.K., Harvey, V.L., Mlynczak, M.G., Funke, B., Garcia-Comas, M., Hervig, M., Kaufmann, M., Kyrola, E., Lopez-Puertas, M., Randall, C.E., Russell III, J.M., Sheese, P.E., Shiotani, M., Skinner, W.R., Suzuki, M., Walker, K.A., 2013. Satellite observations of ozone in the upper mesosphere. J. Geophys. Research 118D, 5803–5821. http://dx.doi.org/10.1002/jgrd.50445.

Smith, A.K., Garcia, R.R., Marsh, D.R., Richter, J.H., 2011. WACCM simulations of the mean circulation and trace species transport in the winter mesosphere. J. Geophys. Res. 116http://dx.doi.org/10.1029/2011JD016083. D20115.

Timofeyev, Y.M., 2016. Study of Atmosphere by a Transparency Method. Nauka, St. Petersburg 367 pages.

Torbin, A.P., Pershin, A.A., Mebel, A.M., Zagidullin, M.V., Heaven, M.C., Azyazov, V.N., 2017. Collisional relaxation of $O_2(a^1\Delta_g$, v = 1, 2, 3) by CO_2. Chem. Phys. Lett. http://dx.doi.org/10.1016/j.cplett.2017.11.052.

Wildt, J., Bednarek, G., Fink, E.H., 1988. Laser excitation of $O_2(b^1\Sigma_g^+$, v = 0, 1, 2) - rates and channels of energy transfer and quenching. Chem. Phys. 122, 463–470.

Yankovsky, V.A., Manuilova, R.O., Babaev, A.S., Feofilov, A.G., Kutepov, A.A., 2011. Model of electronic-vibrational kinetics of the O_3 and O_2 photolysis products in the middle atmosphere: applications to water vapor retrievals from SABER/TIMED 6.3 μm radiance measurements. Int. J. Rem. Sens. 32, 3065–3078. http://dx.doi.org/10.1080/01431161.2010.541506.

Yankovsky, V.A., Martyshenko, K.V., Manuilova, R.O., Feofilov, A.G., 2016. Oxygen dayglow emissions as proxies for atomic oxygen and ozone in the mesosphere and lower thermosphere. J. Mol. Spectrosc. 327, 209–232. http://dx.doi.org/10.1016/j.jms.2016.03.006.

Yankovsky, V.A., Manuilova, R.O., 2017. Retrieval of daytime [O_3] altitude profile from measurements of 1.27 μm O_2 emission in the mesosphere: a comparison of methods. In: Proc. SPIE 10466, 23rd International Symposium on Atmospheric and Ocean Optics: Atmospheric Physics, 1046603, http://dx.doi.org/10.1117/12.2284318.

Yankovsky, V.A., 2017. Proposals on multi-channel methods for the simultaneous remote sensing of [$O(^3P)$], [O_3] and [CO_2] altitude profiles in the mesosphere and lower thermosphere in daytime. Conference Proceedings in J. Aeronaut. Aerospace Eng 6 (2). http://dx.doi.org/10.4172/2168-9792-C1-016.

Yee, J.-H., DeMajistre, R., Morgan, F., 2012. The $O_2(b^1\Sigma_g^+)$ dayglow emissions: application to middle and upper atmosphere remote sensing. Can. J. Phys. 90, 769–784. http://dx.doi.org/10.1139/p2012-073.

Yu, S., Drouin, B.J., Miller, C.E., 2014. High resolution spectral analysis of oxygen. IV. Energy levels, partition sums, band constants, RKR potentials, Franck-Condon factors involving the $X^3\Sigma_g^-$, $a^1\Delta_g$ and $b^1\Sigma_g^+$ states. J. Chem. Phys. 141, 12. http://dx.doi.org/10.1063/1.4900510. 174302.

Yue, J., Russell III, J., Jian, Y., Rezac, L., Garcia, R., López-Puertas, M., Mlynczak, M.G., 2015. Increasing carbon dioxide concentration in the upper atmosphere observed by SABER. Geophys. Res. Lett. 42, 7194–7199. http://dx.doi.org/10.1002/2015GL064696.

Zagidullin, M.V., Khvatov, N.A., Medvedkov, I.A., Tolstov, G.I., Mebel, A.M., Heaven, M.C., Azyazov, V.N., 2017. $O_2(b^1\Sigma_g^+)$ quenching by O_2, CO_2, H_2O, and N_2 at temperatures of 300-800 K. J. Phys. Chem. A121, 7343–7348. http://dx.doi.org/10.1021/acs.jpca.7b07885.